Modelling of the self-assembly of block copolymers in selective solvent

P. Linse

Physical Chemistry 1, Center for Chemistry and Chemical Engineering, Lund University, P.O. Box 124, S-221 00 Lund, Sweden

A number of theories and models with different degrees of sophistication and computational demand are today used to describe the self-assembly of block copolymers in solution. The different types of approach are reviewed and numerical examples are given which demonstrate the applicability of each one. The focus is on approaches useful for long chain molecules in a selective solvent, but illustrations of direct simulations of short-chain molecules are also included.

1. INTRODUCTION

Block copolymers in the melt and in solution tend to self-assemble and form microphases. In the melt and in a nonselective solvent, the repulsive interaction between the monomers on different blocks constitutes the driving force for the process. In a selective solvent, the bad solvency condition for one type of monomer and the good one for the other type is also of importance for the self-assembly. The structure and symmetry of the aggregates formed depend on the relative strength of the interactions as well as on the composition and the architecture of the block copolymer. The aim of the chapter is to present an overview of different theoretical treatments of the self-assembly of block copolymers in a selective solvent. We will cover the range from scaling relations obtained from simplified models to computer intensive simulation approaches. After the introduction where the scope of the overview is given, each type of theory is presented and numerical examples illustrating characteristic results are given. The chapter ends with a summary where the main differences of the types of theory are presented.

The driving force of the self-assembly depends on the particular system. Briefly, amphiphilic block copolymers can be divided into nonionic and ionic block copolymers. In both groups there exist polymers that are soluble in water and in organic solvents. For the nonionic block copolymers, the driving force behind the self-assembly depends on the solvent. In aqueous solution it is normally of entropic origin (e.g. PEO-PPO-PEO), whereas in organic solvents (e.g. PS-PEO) the enthalpic contributions dominate. Obviously, for block polyelectrolytes in aqueous solution and, in particular, for block ionomers in organic solvents, the electrostatic interaction between the free charges plays a dominant role for the self-assembly.

1.1. Scope of the review

A very important area related to the self-assembly of block copolymers in solution is the self-organization of block copolymers in melts. The types of structure appearing, as well as the

theoretical approaches, are often similar in the two areas. Despite the recent advances in the understanding of block copolymers in melt [1], space does not allow to treat these systems. Similarly, the self-assembly of block copolymers in a nonselective solvent displays the same main features as in melts and is hence also treated here superficially. For the same reason, theories developed for describing polymeric gels formed by multifunctional block copolymers are also excluded.

Surfactants (short for surface active agents) constitute an important and related class of molecules. They are short chain molecules with amphiphilic character, and in solution they self-assemble in a manner similar to block copolymers. The driving forces for the self-assembly are the same, but some aspects are different due to the different chain lengths. Hence, the theoretical descriptions of the self-assembly of surfactants and of block copolymers in solution display large similarities, although a number of differences exist. In the following, the scope is on models and theories which have been applied to block copolymer systems. Some of them are the same as those used for describing surfactant systems, but there exist important theories which are only applied to surfactant systems and they are not considered here. However, direct simulation of the self-assembly constitutes the main exception. Due to the shorter chain length, computer simulations of the self-assembly of surfactant systems are simpler (but still not simple), and results pertaining to shorter chains more relevant for surfactant systems will be presented to illustrate what can be modelled for longer chains in the near future. Finally, although kinetic aspects are in many cases of large significance, we will here restrict ourselves to equilibrium systems only.

1.2. Structures and phases

The conventional or classical structures occurring in solutions of block copolymers as well as in solutions of surfactants are spherical, extended cylindrical, and planar aggregates. At low concentration, the spherical aggregates appear as isolated aggregates with no or low spatial correlation. At higher concentration liquid crystalline phases, such as closed packed cubic phases, hexagonal phases, and lamellar phases, may occur. The two former normally exist in two morphologies: a normal one where the solvent constitute the continuous phase and a reverse where the solvent is localized in the interior of the aggregates. Besides the classical structures, recent research has shown that intermediate structures as the double-diamond and the gyroid bicontinuous structures, as well as different perforated lamellae could possibly exist in narrow concentration and temperature ranges.

A large fraction of the theoretical effort has been devoted to describe the onset of forming the spherical aggregates, normally referred to as micelles. In particular, the lowest copolymer concentration at which micelles exist (the critical micellar concentration, cmc) is of large interest, but also the sizes of the micellar core and corona (the latter is also referred to as shell or brush height), the concentration of nonassemblied copolymers above the cmc, and the ordered phases occurring at high concentrations are of great interest to describe.

1.3. Types of theory

The different theories and models are presented in order of increasing computational demand. The theories are divided in (i) scaling approaches, (ii) semi-analytic mean-field models, (iii) numerical self-consistent mean-field models, and (iv) simulation approaches. The above division is of course somewhat arbitrary, and the borders between the subdivisions are not sharp.

The scaling approach provides us with simple but useful relations of how, e.g., the size of the micellar core and corona depends on the number of segments of the different blocks. The word segment is used to denote a part of a chain in the model and it has to be mapped on a monomer, repetitive unit, or similar, when the theory is applied. In the semi-analytic mean-field models, one normally assumes some block profile and from an expression for the free energy contributions, the aggregation number, the cmc, and the phase diagram can be extracted. The starting point of the numerical self-consistent mean-field models is normally random walks which represent the configurations of the chain molecules. These walks are performed in a potential field which, as such, depends on the configurations of the molecules. In addition to the results of the semi-analytic mean-field models, volume fraction profiles, distribution of segments, etc., are obtained. Finally, through direct simulations it is possible to go beyond the mean-field approximation, but the computational demand is high for polymeric systems.

2. SCALING APPROACHES

The idea behind the scaling "anzats" is to obtain relations which predict how quantities of interest depend on other variables without a full knowledge of the dependencies on all variables. On the basis of some simple model of the system, the leading free energy contributions are formulated. After minimization of the free energy with respect to one or a few variables, the leading dependencies of these quantities on the other variables are often readily extracted.

2.1. Micellization of AB-diblock copolymers in a selective solvent

We will consider first a solution of a monodisperse AB-diblock copolymer in a selective solvent of low molecular weight. The number of segments of the copolymer blocks are represented by N_A and N_B, respectively. We will derive the scaling relations of the size and the aggregation number of the micelles formed. Two limiting cases will be considered: the large core case [2] valid when $N_A >> N_B$ ("crew cut micelles") and the small core case [3,4] for $N_A << N_B$ ("hairy micelles"). In the former limit the analogy with theories for polymer brushes [2] is used, whereas in the latter case the theory is developed from star polymer theory [5,6].

The micelles are assumed to be monodisperse and their concentration so low that micelle-micelle interaction are negligible. A micelle is modelled as two concentrical spherical regions, where the molten lyophobic A-blocks reside in the central core, whereas the B-blocks, swollen by the solvent, are located in the shell. The incompatibility between the two types of blocks is assumed to be large so the core-shell interface, at which the AB junctions are localized, is sharp. In the case of the large core, the volume fraction of B segments is treated as constant in the shell (model I) (not always a realistic assumption, but nevertheless made), whereas in the case of the small core, the volume fraction of B segments is allowed to decay with increasing distance (model II), (see Figure 1).

Assuming that the core is incompressible and consists only of A segments, i.e, $\phi_A^{core} = 1$, we obtain the scaling relation

$$R_A^3 \approx pN_A a^3 \tag{2.1}$$

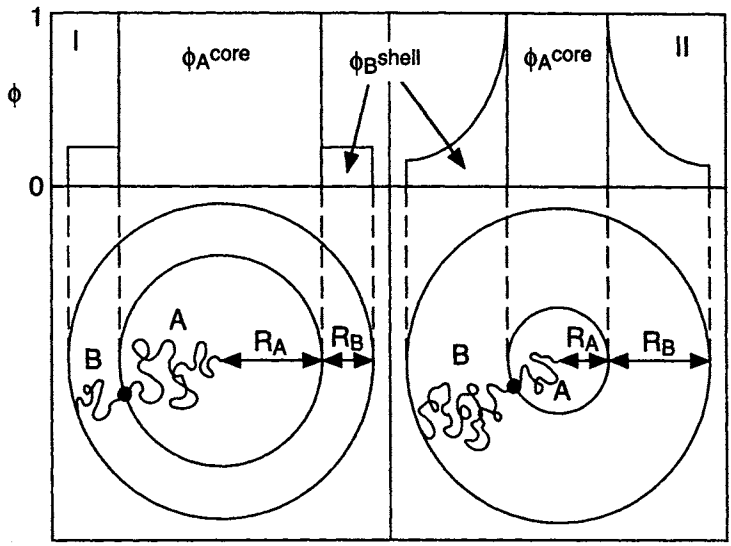

Figure 1. Illustration of model I (left) and II (right) of the AB-diblock copolymer micelle in a selective solvent (lower panel) and the volume fraction profiles of the polymer blocks (upper panel) applied for the large core case ($N_A >> N_B$) and the small core case ($N_A << N_B$), respectively.

where p denotes the aggregation number and a the length of a segment. (The symbol $\approx$ denotes equal within a numerical factor of order one.)

For model II, the scaling relation for R_B is obtained by analysing the conformations of the B-blocks in terms of blobs [7]. With the following assumptions: (i) the shell region consists of concentrical shells of blobs, (ii) there are p blobs in each shell, (iii) the blobs size ξ depends only on r, and (iv) the B-segments are in a good solvent, the volume fraction of the B segments can explicitly be expressed as $\phi_B^{shell} \approx p^{2/3}(r/a)^{-4/3}$. By integration of ϕ_B^{shell}, the scaling relation

$$R_B \approx p^{1/5} N_B^{3/5} a \qquad \text{(model II)} \qquad (2.2')$$

is obtained after applying $R_A << R_B$.

The two dominant contributions to the free energy are assumed to be the interfacial tension (enthalpic) and the chain stretching (entropic). Thus, the total free energy of a micelle is approximated according to

$$F = F_{interface} + F_{def}^{core} + F_{def}^{shell} \qquad (2.3)$$

where $F_{interface}$ describes the interfacial free energy, F_{def}^{core} the stretching free energy of the A-

blocks, and F_{def}^{shell} the corresponding quantity for the B-blocks. The interfacial free energy is assumed to be proportional to the area of the interface, thus

$$F_{interface} \approx \gamma R_A^2 \tag{2.4}$$

where γ is the surface tension. In this simple approach, the A blocks are assumed to be uniformly stretched with an end-to-end distance equal to the core radius, R_A, (obviously not a fully realistic picture) and the accompanied cost is expressed as

$$\beta F_{def}^{core} \approx p\left(\frac{R_A}{N_A^{1/2}a}\right)^2 \tag{2.5}$$

where $\beta = 1/(kT)$ with k being Boltzmann's constant and T the temperature. In model I, a constant volume fraction of the B block is assumed and the uniformly stretching assumption gives similarly

$$\beta F_{def}^{shell} \approx p\left(\frac{R_B}{N_B^{1/2}a}\right)^2 \qquad \text{(model I)} \tag{2.6}$$

Regarding model II, the blob picture is used again. To the leading order there are $\approx p^{1/2}$ blobs per chain and with a free energy penalty of kT per blob due to the confinement of the B-blocks at the core surface, we get

$$\beta F_{def}^{shell} \approx p^{3/2} \qquad \text{(model II)} \tag{2.6'}$$

Substitution of eqs (2.4)-(2.6) in eq (2.3) and elimination of R_A and R_B by employing eqs (2.1)-(2.2) leads to a free energy expression of a single micelle where the aggregation number p is the only unknown parameter according to

$$\beta F \approx \gamma N_A^{2/3} p^{2/3} a^2 + N_A^{-1/3} p^{5/3}(1 + N_A^{-1} N_B \rho^{-2}) \qquad \text{(model I)} \tag{2.7}$$

$$\beta F \approx \gamma N_A^{2/3} p^{2/3} a^2 + N_A^{-1/3} p^{5/3} + p^{3/2} \qquad \text{(model II)} \tag{2.7'}$$

The aggregation number can now determined by minimization of the free energy per polymer chain, F/p. For the case of large cores (model I), the following scaling relations are obtained:

$$p \approx \gamma N_A \tag{2.8}$$

$$R_A \approx \gamma^{1/3} N_A^{2/3} a \tag{2.9}$$

where $N_A >> N_B$ has been applied corresponding to $F_{def}^{core} >> F_{def}^{shell}$. In the opposite limit with small cores (model II), we obtain:

$$p \approx \gamma^{6/5} N_A^{4/5} \tag{2.8'}$$

$$R_A \approx \gamma^{2/5} N_A^{3/5} a \tag{2.9'}$$

$$R_B \approx \gamma^{6/25} N_A^{4/25} N_B^{3/5} a \tag{2.10'}$$

where $(N_A^{-2}p)^{1/6} << 1$ has been used corresponding to $F_{def}^{core} << F_{def}^{shell}$.

Thus, in the large core limit, the aggregation number is determined from the balance of the deformation free energy in the core and the interfacial free energy; the former tending to reduce p and the latter tending to increase p. Hence, the assumption of constant volume fraction in the shell does not affect the scaling relations, at least to the leading order. In the small core limit, the limitation of the growth of the micelle is, however, governed by the increased free energy of the blocks in the shell instead of in the core.

2.2. Solubilization in block copolymer micelles

The self-assembly of the block copolymers creates an environment in the core which is different from that in the solution. Solutes not soluble in the solvent can be solubilized (dissolved) in the core, and hence the solubility of a solute in a system can significantly be enhanced by the presence of block copolymers.

The blob picture of star polymers [5,6] has been employed by Nagarajan and Ganesh for deriving scaling relations where small and lyophobic molecules are solubilized in the micellar core [8]. Their extension involves the cases where the the lyophobic segments are nonswollen or swollen by the solubilizate leading to a radial volume fraction profile in the core according to $\phi_A^{core} = r^{-1}$ or $r^{-4/3}$, respectively. The corresponding incompressibility assumption of the core gives

$$R_A^3 \approx p N_A a^3 \langle \phi_A^{core} \rangle \tag{2.11}$$

where $\langle \phi_A^{core} \rangle$ denotes the average volume fraction of A in the core. With the assumption of unaffected surface tension due to the solubilization (for simplicity), the following scaling relations are obtained:

$$p \approx \gamma N_A \tag{2.12}$$

$$R_A \approx \gamma^{1/4} N_A^{3/4} a \tag{2.13}$$

$$R_B \approx \gamma^{1/5} N_A^{1/5} N_B^{3/5} a \tag{2.14}$$

for $\phi_A^{core} = r^{-1}$ and

$$p \approx \gamma^{10/11} N_A^{12/11} \tag{2.15}$$

$$R_A \approx \gamma^{2/11} N_A^{9/11} a \tag{2.16}$$

$$R_B \approx \gamma^{2/11} N_A^{12/55} N_B^{3/5} a \tag{2.17}$$

for $\phi_A^{core} = r^{-4/3}$, both in the limit of $R_A >> R_B$.

Thus, for "hairy" micelles the scaling approach predicts that the solubilization causes the aggregation number as well as the core and shell dimensions to depend stronger on N_A and weaker on γ than without solubilization.

2.3. Micellization of polyelectrolytes

An extension of the scaling relations for the small core limit to the case where the B-block is charged has been given by Dan and Tirrell [9]. With the assumption that the salt concentration is sufficiently high such that the persistence length of the B block is smaller than the blob size, the previous blob picture remains. In this regime, the leading terms of p and R_A are found to be independent of the salt concentration ϕ_{salt}, whereas the shell thickness scales as

$$R_B \approx \gamma^{6/25} N_A^{4/25} N_B^{3/5} \phi_{salt}^{-2/5} a \tag{2.18}$$

At low salt concentrations, where the persistence length exceeds the blob size, it is anticipated that both p and R_A display salt dependence.

3. SEMI-ANALYTIC MEAN-FIELD MODELS

The basic idea behind the core-shell models is the assumed physical separation of the two different types of blocks of the copolymer into two domains, the core and the shell (corona) of the micelle. On the basis of this separation, a free energy expression is constructed which represents the free energy of the micelle with respect to some reference state. The final step involves a minimization of the free energy with respect to a few parameters characterizing the micellar aggregate (as the domain sizes and the micellar volume fraction). In the case of only a few free energy terms, the simple scaling relations of the size of the domains are recovered.

3.1. Micellization of AB-diblock copolymers

The main variation within this class of models lies in the selection of free energy terms which describe different aspects of the self-assembly. In an early contribution, de Gennes [2] considered three terms: (i) the interfacial energy between the core and the corona, (ii) the deformation free energy of the A-block, and (iii) the deformation free energy of the B-block. The subsequent extension of Leibler et al. [10] included terms describing the mixing entropy of the solvent and the lyophobic block, the mixing entropy of micelles with solvent and non-assembled block copolymers, and the free energy of the homogeneous reference solution. Later Munch and Gast [11] extended the same theory to copolymer with different block sizes, and they also investigated the phase equilibrium between micelles and lamellar phases. Independently of Leibler et al., Noolandi and coworkers [12,13] developed very similar theories utilizing slightly different free energy expressions and obtained essentially the same results. In particular, they used a more elaborate model for obtaining the interfacial free energy, and they also included a term representing the free energy penalty of confining the A-B junctions.

In order to illustrate the principles of the core-shell model in more detail, the approach by Leibler et al. [10] and later used by Much and Gast [11] will be presented here, slightly reformulated.

The micellar solution is divided into spherical cells, each containing one spherical micelle with its accompanying solution. The volume of the cell is the inverse of the micellar number density. The lyophobic A-block constitutes the micellar core, whereas the shell contains the lyophilic B-block swollen with solvent as shown in Figure 2. The third region contains non-assembled (referred to as free) block copolymers and solvent. The notations used for the volumes of the three regions, the radius of the core, the thickness of the shell, and the volume fractions are also shown in Figure 2. The number of segments of the copolymer blocks are represented by N_A and N_B, respectively, and that of the solvent by N_S. All segments have the same length, a, and the same volume, a^3. The various interactions are described by Flory-Huggins χ-parameters [14]. For simplicity, the B segments and the solvent molecules are identical, i.e, $\chi_{BS}= 0$ and $\chi_{AB} = \chi_{AS}$, and hence the systems is characterized by only one interaction parameter, viz. χ.

The free energy of a single cell is expressed as

$$F = (F_{interface} + F_{def} - TS_{mix}^{shell}) + F_{mix}^{free} - TS_{mix}^{micelle} \tag{3.1}$$

where the terms in parentheses represent the free energy of a single micelle fixed in space. The first term in eq (3.1) denotes the interfacial free energy of the interface between the core composed by A-segments and the shell composed by B-segments and solvent which is given by

$$F_{interface} = 4\pi R_A^2 \gamma \tag{3.2}$$

where $\gamma = kT\,(\chi/6)^{1/2}$ [15]. The second contribution arises from the elastic deformation of the copolymers in the micelle. It is assumed that all A-blocks are uniformly stretched/compressed from their Gaussian behaviour to an end-to-end distance equal to R_A and similarly for the B-blocks. Leibler et al. [10] employed

$$\beta F_{def} = \frac{3}{2} p \left[\left(\frac{R_A}{N_A^{1/2} a} \right)^2 + \left(\frac{R_A}{N_A^{1/2} a} \right)^{-2} + \left(\frac{R_B}{N_B^{1/2} a} \right)^2 + \left(\frac{R_B}{N_B^{1/2} a} \right)^{-2} - 4 \right] \tag{3.3}$$

where p is the number of copolymers in the micelle. The following term in eq (3.1) represents the mixing free energy of solvent molecules with the B-segments in the shell

$$-S_{mix}^{shell}/k = \frac{V^{shell}}{a^3} \left[\frac{1}{N_S} \phi_S^{shell} \ln(\phi_S^{shell}) \right] \tag{3.4}$$

Finally, the remaining two terms in eq (3.1) arise from the free energy of the homogeneous solution outside the micelles and the free energy of mixing the micellar aggregates in the micellar solution. Using Flory-Huggins mean-field model of homogeneous polymer solutions

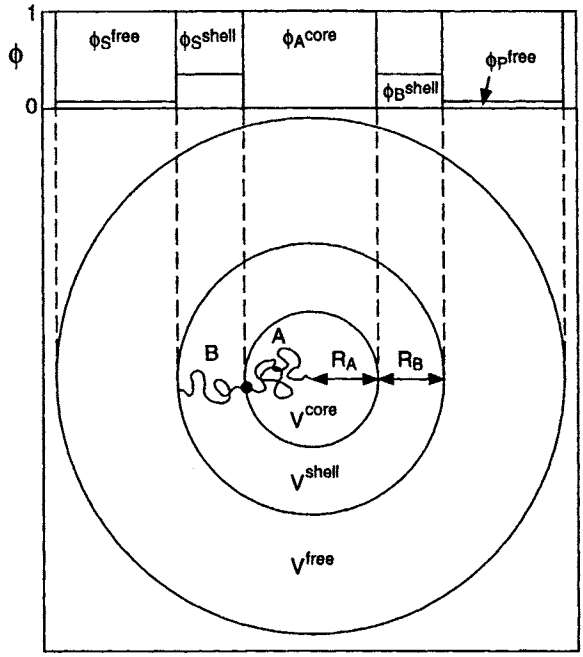

Figure 2. Illustration of the model showing the core and shell regions of a spherical micelle composed by an AB-diblock copolymer and the surrounding homogeneous polymer solution (lower panel). The volume fractions of the components in the three uniform regions are also displayed (upper panel).

[14], the former of the two is expressed as

$$\beta F_{mix}^{free} = \frac{V^{free}}{a^3}\left[\frac{1}{N_A+N_B}\phi_P^{free}\ln(\phi_P^{free}) + \frac{1}{N_S}\phi_S^{free}\ln(\phi_S^{free}) + \chi\phi_A^{free}(\phi_B^{free}+\phi_S^{free})\right] \tag{3.5}$$

where $\phi_A^{free} = N_A/(N_A+N_B)\phi_P^{free}$ and similarly for ϕ_B^{free}. The latter term is represented by

$$-S_{mix}^{micelle}/k = \phi_M^{-1}[\phi_M \ln(\phi_M) + (1-\phi_M)\ln(1-\phi_M)] \tag{3.6}$$

where $\phi_M = V^M/V$ denotes the micellar volume fraction with $V^M = V^{core} + V^{shell}$ and $V = V^M + V^{free}$. By employing the incompressibillity relations $V^{core} = (4\pi/3)R_A^3 = pN_Aa^3$, $V^{shell} = (4\pi/3)[(R_A+R_B)^3] - R_A^3 = pN_Ba^3/\phi_B^{shell}$, and $\phi_P^{free}V^{free} = \phi_P V - p(N_A+N_B)a^3$ as well as the fact that that volume fractions should sum up to one, F can be expressed in only three independent variables. For numerical computation, p (the aggregation number), ϕ_B^{shell} (the volume fraction of B segments in the shell), and ϕ_P^{free} (the volume fraction of free polymers) form a convenient set.

After minimization of F with respect of these variables, the equilibrium properties of the micellar solution of this model are obtained. In the original reports [10,11], the three coupled

nonlinear equations obtained after partial differentiation were solved; however direct minimization is more straightforward and works fine.

3.2. Triblock copolymers

Extensions of the core-shell theory to cover cases with ABA-triblock copolymers have been proposed [16-18]. The main additional contribution is the cost for the middle block to form a loop. Ten Brinke and Hadziioannou [16] used the term $(3/2)\beta_l kT\ln(N_{loop})$ per polymer chain, where $\beta_l \approx 1$ and N_{loop} is the length of looping middle block. Later, Balsara et al. [17] suggested a smaller free energy cost, $(1/2)kT\ln(\pi\chi N_{loop})$, as the leading term. The general result is that the triblock copolymer displays an increased cmc as compared to a diblock copolymer with same A/B ratio and with half molecular mass. Balsara et al. [17] showed that the two cases lead to considerably differing increases in the cmc as compared to no loop formation. Recently, ordered structures occurring in ABC-triblock copolymers have received increasing attention [19,20]. A large number of possible morphologies have been suggested in melt and the these ideas should also hold for ABC-triblock copolymers in solution.

3.3. Polydisperse and mixed micelles

In the description so far, only monodisperse micelles have been considered. By utilizing theories developed for the self-assembly of short chain surfactants, Nagarajan and Ganesh [21] proposed a theory which contains micelles of all possible sizes beside the solvent molecules and singly dispersed copolymer molecules (unimers). The minimization of the free energy of this multicomponent system leads to an expression for the equilibrium size distribution of the micelles. Similarly, Gao and Eisenberg adapted a slightly different theory of describing the micellization of surfactants to the micellization of block copolymers [22].

The case of a mixture of two different diblock copolymers has been examined by Marques and coworkers [23,24]. For many conditions only mixed micelles are formed, but they also found situations where mixed micelles coexist with micelles formed by only one of the copolymers.

3.4. Solubilization

Nagarajan and Ganesh have also considered the case where lyophobic molecules are solubilized in the core of the micelles [25]. They found that the width of the distribution of the aggregation number is normally of minor consequence, and similarly the variation of the number of solutes in the micelles is small. The solubilization increases the aggregation number of the micelle and strongly increases the amount of solutes able to be dissolved in the phase. The effect of chain architecture on the solubilization has also bee examined [26].

3.5. Polyelectrolytes

Marko and Robin have derived expressions for the cmc as well as for the micellar size and aggregation number at the cmc for an AB block copolymer where A is insoluble and B is charged [27]. They used a similar approach as in section 3.1, but employed different free energy contributions. In particular, the driving force of the micellization is the bad solvency of the A block, which is opposed by the electrostatic repulsion within and among the charged blocks.

3.6. Selected results

The type of predictions obtained from the core-shell model, as described in section 3.1, will be illustrated for a symmetric diblock copolymer with $N_A = N_B = 50$ in a solvent with $N_S = 1$. The corresponding results of the more extended self-consistent lattice mean-field lattice theory (to be presented in section 4 below) are also included.

The volume fraction of free polymers (in the micellar free solution) and the volume fraction of micelles as a function of the total polymer volume fraction at $\chi = 1.45$ is given in Figure 3. At sufficiently low polymer volume fractions, the global free energy, as expressed by eqs (3.1)-(3.6), is obtained for $\phi_M \equiv 0$, i.e., there is only a homogeneous polymer solution without any micelles. However, at increasing ϕ_P, the global minimum occurs now for $\phi_M > 0$, hence micelles are present. The volume fraction where this transition occurs is referred to as the critical micellar concentration, and $\phi_P^{cmc} \approx 10^{-5}$ for the present parameter values. Above ϕ_P^{cmc}, the volume fraction of free polymers is almost constant; ϕ_P^{free} increases only 10% when ϕ_P increases 1000-fold.

Figure 4 shows that also the predicted aggregation number p is essentially independent of the polymer volume fraction and equals to ca. 55. The other parameter characterizing the micelle, ϕ_B^{shell}, is even less sensitive to ϕ_P. The weak influence of ϕ_P on p and ϕ_B^{shell} makes it possible to simplify the determination of these quantities by only considering the first three terms in eq (3.1) [10]. However, in order to determine ϕ_P^{cmc} and ϕ_P^{free}, the full expression is needed. Above the cmc, there is a partitioning of the polymers between the micelles and the intervening solution. Figure 4 also shows that the fraction of self-assembled block copolymers increases after the cmc to reach 90% at $\phi_P \approx 10\phi_P^{cmc}$.

The extension of the micellar core, the thickness of the shell, and the volume fraction of solvent in the shell are also of large interest. These quantities are shown in Figure 5 in terms of radial volume fraction profiles. For the present system, the core extends nearly 9 length units and the shell is 10.4 length units wide. Thus, both blocks are extended beyond their random coil configurations. The shell is highly swollen; ϕ_B^{shell} is only ca. 11%.

The degree of incompatibility between the A-segments on the one hand and the B-segments and solvent molecules on the other should affect the cmc. Figure 6 shows that the cmc is indeed very sensitive to χ. An increase of χ from 1.3 to 1.5 reduces ϕ_P^{cmc} from 10^{-2} to 10^{-6}. The rather high value of $N_A\chi$ ($\approx$65) required to obtain micelles in a solution of small molecules is related to the large loss in mixing entropy of the solution upon micellization. Already at $N_S = 5$, it is sufficient with $\chi = 0.435$ ($N_A\chi = 22$) to obtain $\phi_P^{cmc} = 10^{-2}$. As N_S is increased, the penetration of the solvent into the shell region is reduced as demonstrated by an increased ϕ_B^{shell} and a reduced shell thickness, which leads to less stretched B-blocks.

4. NUMERICAL SELF-CONSISTENT MEAN-FIELD MODELS

Mean-field descriptions of inhomogeneous systems containing chain molecules have been developed along two main directions. A lattice version was developed by Scheutjens and Fleer [28] from the earlier work by Flory [14]. It has been widely used to model adsorption at interfaces [29] and self-assembly of chain molecules (surfactants and polymers). Independently

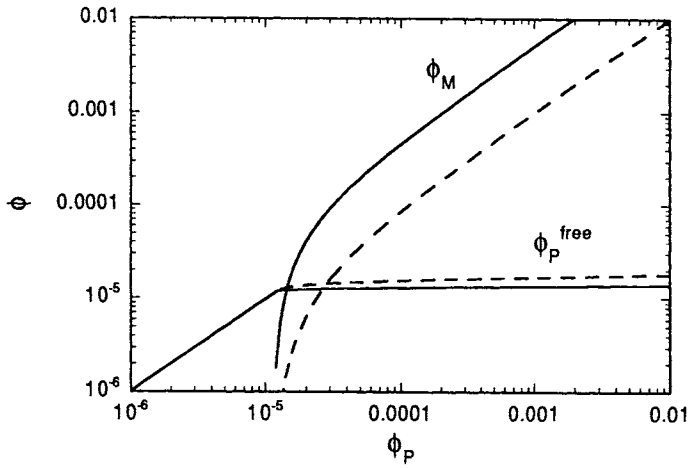

Figure 3. Volume fraction of free polymers ϕ_P^{free} and of micelles ϕ_M as a function of the total polymer volume fraction ϕ_P for a diblock copolymer with $N_A = N_B = 50$ and $N_S = 1$ from the core-shell model with $\chi = 1.45$ (solid curves) and the lattice mean-field theory with $\chi = 1.24$ and a hexagonal closed-packed lattice (dashed curves). Different values of χ were selected to give the same cmc. (In the core-shell model, ϕ_P^{free} refers to the volume fraction in the micellar free subvolume.)

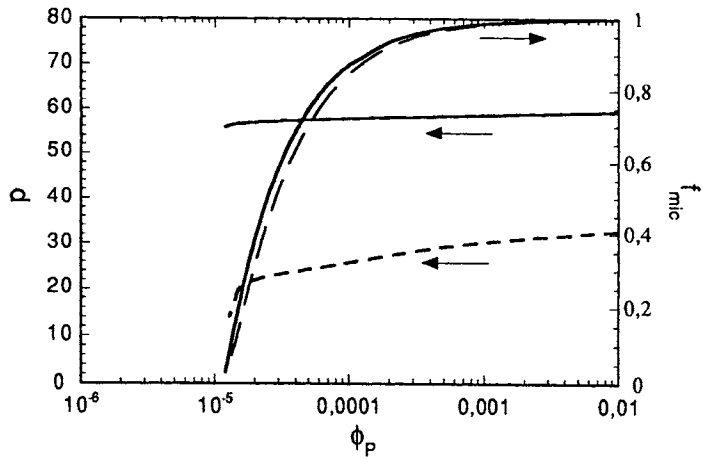

Figure 4. Aggregation number p (left axis) and fraction of polymers in micelles (right axis) as a function of the total polymer volume fraction ϕ_P for a diblock copolymer with $N_A = N_B = 50$ and $N_S = 1$ from the core-shell model with $\chi = 1.45$ (solid curves) and the lattice mean-field theory with $\chi = 1.24$ and a hexagonal closed-packed lattice (dashed curves).

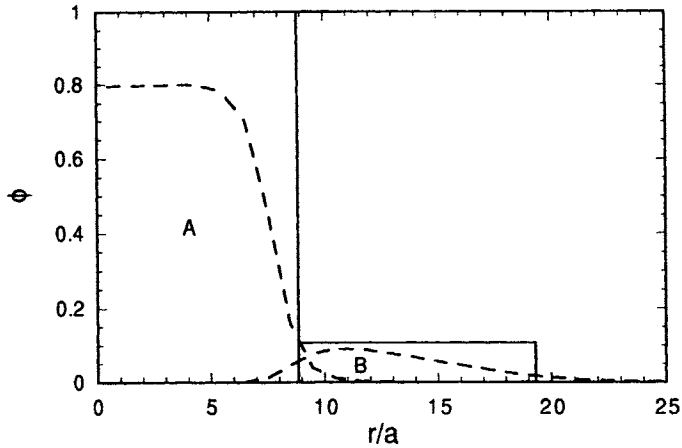

Figure 5. Volume fraction profiles of the A and B segments for a diblock copolymer with $N_A = N_B = 50$ and $N_S = 1$ at $\phi_p = 10^{-3}$ from the core-shell model with $\chi = 1.45$ (solid curves) and the lattice mean-field theory with $\chi = 1.24$ and a hexagonal closed-packed lattice (dashed curves). The radial distance is given in reduced units (segment lengths).

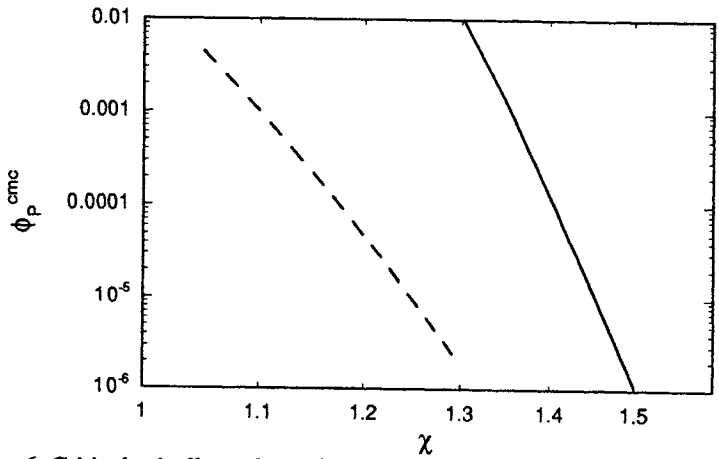

Figure 6. Critical micellar volume fraction as a function of the interaction parameter χ for a diblock copolymer with $N_A = N_B = 50$ and $N_S = 1$ from the core-shell model (solid curves) and the lattice mean-field theory with a hexagonal closed-packed lattice (dashed curves).

and in parallel, the corresponding continuum version, as derived from the functional integral formalism [30], has been described by Hong and Noolandi [31] and utilized in a number of investigations, in particular of block copolymers at fluid interfaces. Recently, both approaches were applied to the same model system and were compared directly [32]. Both approaches are presented below by using, as far as possible, equivalent expressions to highlight their similarities. For simplicity, only the case of the homopolymers is considered, but both approaches are readily generalized to copolymers [33].

4.1. Lattice approach

The division of the space into lattice sites, which are occupied by a solvent molecules or a segment of a chain molecule is fundamental in the lattice approach. Normally, spatial inhomogeneities are permitted in one direction and the random-mixing approximation is applied to all sites in each layer separately. The number of nearest neighbour sites, z, is determined from the lattice topology. A chain molecule is described as a connective walk on the lattice. The relative degeneration of a component x in conformation c is given by

$$\omega_{xc} = L_{s=1} \prod_{s=2}^{r_x} \lambda^{(s)} \tag{4.1}$$

where $L_{s=1}$ denotes the number of equivalent starting positions, $\lambda^{(s)}$ is a simplified notation for the transition probability of a random walk from the site where segment s-1 is located to the site where segment s is located, and is r_x the number of segments of component x.

The free energy expression of the system is given by

$$\beta(A-A^*) = \sum_x \sum_c n_{xc} \ln \frac{n_{xc} r_x}{\omega_{xc}} + \frac{1}{2} \sum_i L_i \sum_x \sum_{x'} \phi_{xi} \chi_{xx'} \langle \phi_{'xi} \rangle \tag{4.2}$$

where the first factor represents the entropy and the latter the interaction among the segments of the different components using Flory-Huggins interaction parameter χ. In eq (4.2), n_{xc} denotes the number of molecules of type x in conformation c, L_i the number of sites in layer i, and <...> an average over layer i-1, i, and i+1. From the maximization of the partition function (minimization of the free energy) with respect to the set of all conformations $\{n_{xc}\}$ under the constraint of filled lattice sites, the distribution of segment s of component x in layer i can be expressed by

$$n_{xsi} = \left\{ \frac{n_x}{\mathbf{s}^T.(\mathbf{W})^{r_x-1}.\mathbf{p}(x,1)} \right\} \{\mathbf{s}^T.(\mathbf{W})^{r_x-1}.\Delta_i\} \{\Delta_i^T.(\mathbf{W})^{s-1}.\mathbf{p}(x,1)\} \tag{4.3}$$

where the first factor is a normalization factor assuring that n_x molecules of type x is present. The last factor denotes the number of chains of type x with the start distribution $\mathbf{p}(x,1)$ among the layers which has its s:th segment in layer i and the second factor gives the appropriate

weight of the remaining part of the chain to be somewhere on the lattice. In eq (4.3), W is a tridiagonal matrix comprising elements which contains factors describing the lattice topology and factors containing the mean-field potential for segments of component x, $\Delta_i^T = (0, ..., 0, 1, 0, ..., 0)$, and $\mathbf{s}^T = (1, 1, ...,1)$. The number of segments of component x in layer i is given by $n_{xi} = \sum_{s=1}^{r_x} n_{xsi}$. Finally, the volume fraction in a layer, ϕ, is obtained by diving n_{xsi} and n_{xi} by the number of lattice sites in that layer.

4.2. Continuum approach

In the continuum description, the partition function for a multicomponent system can be expressed as a functional integral over all space curves representing all chain molecules. Following Hong and Noolandi [31], the probability functional for a given space curve $P[\mathbf{r}_x(\bullet)]$ of a flexible chain molecules of type x (component x) is assumed to be of the Wiener form, i.e.,

$$P[\mathbf{r}_x(\bullet)] \propto \exp\left[-\frac{3}{2b^2}\int_0^{r_x} dt\, \dot{\mathbf{r}}_x^2(t)\right] \tag{4.4}$$

b being the Kuhn segment length of a chain and r_x the number of statistical segments. In an (external) field the distribution function of component x with one end at $\mathbf{r}_0$ and the other at $\mathbf{r}$ is given by the Green function $Q_x(\mathbf{r}, r_x \mid \mathbf{r}_0)$, which satisfies the modified diffusion equation

$$\frac{\partial Q_x}{\partial t} = \frac{b^2}{6}\nabla^2 Q_x - \omega_x Q_x \tag{4.5}$$

with $Q_x(\mathbf{r}, 0 \mid \mathbf{r}_0) = \delta(\mathbf{r} - \mathbf{r}_0)$, where $\omega_x[\mathbf{r}_x(t)]$ is the external potential.

From a free energy functional involving entropic terms (of the type $\rho_x(\mathbf{r}) \ln \rho_x(\mathbf{r})$, where $\rho_x(\mathbf{r})$ denotes the segment number density of component x at $\mathbf{r}$) and enthalpic terms (of the type $\rho_x(\mathbf{r})\rho_{x'}(\mathbf{r})\chi_{xx'}$, where $\chi_{xx'}$ is the Flory-Huggins interaction parameter between segments in components x and x'), minimization of the partition function with the constraint of constant local density gives the mean-field potential above denoted as an external potential.

From the Green functions, all relevant properties can be calculated. The density of segments of rank t of component x, $\rho_x(\mathbf{r},t)$, is, e.g., given by

$$\rho_x(\mathbf{r},t) = \left\{\frac{n_x}{\int d\mathbf{r}\int d\mathbf{r}_0 Q_x(\mathbf{r},r_x|\mathbf{r}_0)}\right\}\left\{\int d\mathbf{r}_0 Q_x(\mathbf{r},r_x-t\,|\mathbf{r}_0)\right\}\left\{\int d\mathbf{r}_0 Q_x(\mathbf{r},t\,|\mathbf{r}_0)\right\} \tag{4.6}$$

where the three factors have exactly the corresponding meaning as in eq (4.3). By integration over t, the polymer density $\rho_x(\mathbf{r})$ (equivalent to n_{xi}) is readily obtained from eq (4.6).

Thus, from the specification of the chain molecules in terms of their sequence of different types of segments and the interaction among all pairs of segment types, the distribution of the different segments in the inhomogeneous system is available. The calculations can be performed either with a specified number of components $\{n_x\}$ as indicated above, or the inhomogeneous system can be in equilibrium with a bulk of specified composition.

The main difference between the lattice and continuum approaches is the description of the chain conformations. In the lattice theory, these are relatively few due to the restriction to a lattice, whereas in the continuum theory they are infinite. However, the discretization of the equations makes the number of conformations finite, and in the limit of a mesh size of the discretization equal to the lattice size the approaches are essentially the same. Still, for more complex geometries, the continuum approach seems to be more tractable [19].

4.3. Different extensions

Over the years, the lattice approach has been extended to include, e.g., (i) charged components, (ii) branched components, (iii) bond angle restrictions, and (iv) the exclusion of direct backfolding [29]. Moreover, both the lattice and the continuum approaches have been applied to curved geometries and to the case where the segments have internal degrees of freedom. The latter extension has been very fruitful for modeling the reduced solubility of, e.g., poly(ethylene oxide) (PEO) in polar solvent [32,34-40], and has been used for modeling titrating polyelectrolytes [41].

4.4. Selected results

Some illustrative predictions of the self-assembly of $A_{50}B_{50}$ block copolymers in monomeric and selective solvent from the lattice theory were given in Figures 3-5. The qualitative predictions from the core-shell and the numerical self-consistent mean-field lattice approaches are the same. However, some major differences are discernable: (i) the cmc depends differently on χ due to different descriptions (free energy terms) of the system, (ii) compared for the same cmc (by selecting different χ-values), different aggregation numbers are predicted, and (iii) the lattice approach *predicts* an A-B separation where the interfacial width is substantial (for this model system).

Radial volume fraction profiles for a more "hairy" polymeric micelle formed by $A_{50}B_{500}$ block copolymers in solution are shown in Figure 7. The central lyophobic core of A segments is well represented by a block profile, whereas the lyophilic B segments form a highly solvated corona. Further analyses of Leermakers et al. [42] suggested a division of the profile of the B segments into four parts: (i) the "proximal" one where B segments are adsorbed onto the core, (ii) the "central" one where a power law regime exists, (iii) a "parabolic-like" regime further out and finally (iv) a "distal" regime where the profile approaches the bulk value approximately exponentially (cf. inset of Figure 7). Thus, such model calculations can provide guidance as to how to select profiles in more simple theories/models and in the evaluation of scattering experiments.

Since the free energy of the system and the chemical potentials of the components are available, we are also able to predict the stability of different ordered phases relatively to each other and to the disordered (homogeneous) one. By calculating the stability of phases with different structures, we can predict a phase diagram that contains different ordered phases. Figure 8 shows the prediction of such a phase diagram for the $(EO)_{21}(PO)_{47}(EO)_{21}$ triblock copolymer (Pluronic P94) in aqueous solution, made by Noolandi et al. [32]. At low polymer volume fraction we have the disordered L_1 phase. At increasing polymer concentration there are successive transitions to a cubic lattice of packed spherical aggregates (I_1), hexagonally packed cylindrical aggregates (H_1), and lamellar aggregates (L_α). At even higher concentrations the reverse phases appear where the water is localized in the center of the cylindrical aggregates

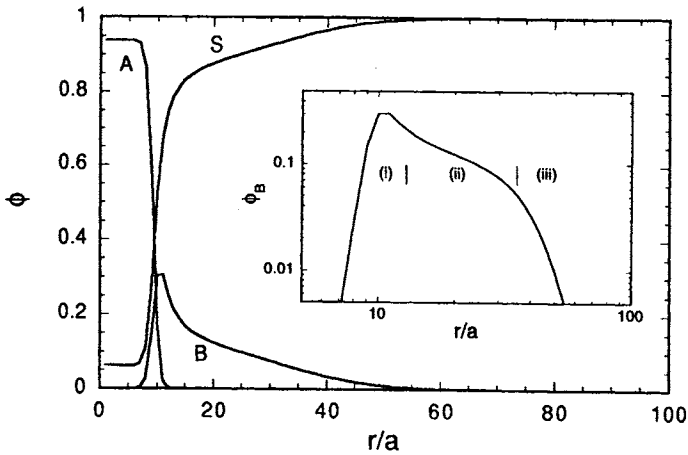

Figure 7. Radial volume fraction profiles of A and B segments and solvent through a spherical micelle of $A_{50}B_{500}$ molecules for $\chi_{AB} = \chi_{BS} = 0.5$, $\chi_{AS} = 2.0$, and $N_{agg} = 54$ using a face centered cubic lattice. The inset shows the profile of the B segments in a log-log representation and the extension of the different regions are indicated. The profile for the "distal" region is not visible.

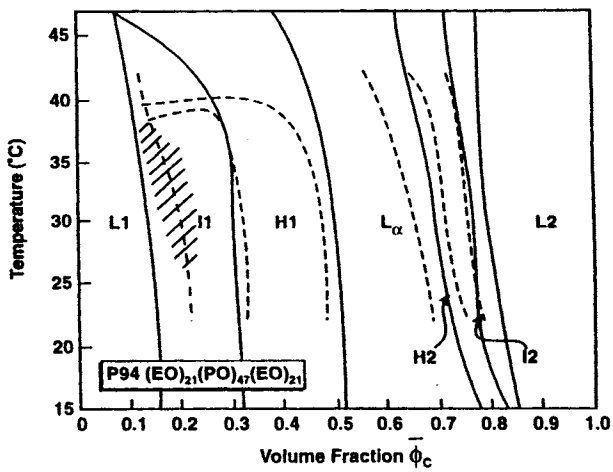

Figure 8. Calculated phase diagram for $(EO)_{21}(PO)_{47}(EO)_{21}$ in aqueous solution using the continuum (solid) and the lattice (dashed) descriptions. The hatched area shows the region with disordered solution of micelles. (Reprinted with permission from ref [32]. Copyright 1996 American Chemical Society.)

(H_2) and in the center of the reversed packed micelles (I_2). Finally, at very high polymer concentrations a new disordered phase appears (L_2). The two-phase regions between the one-phase regions were not considered. At increasing temperature the solubility of the polymer is reduced, promoting a change in the stability of the phases towards less curved surfaces (defined with water on the outside). Although the lattice and continuum approaches give slightly different phase boundaries, the general appearance is the same. The phase boundaries predicted by the two numerical methods seem to approach each other as the polymer chains becomes longer [32]. By using the theory of thermodynamics for small systems [43], a prediction of the cmc in the disordered L_1 phase can be made. The hatched area in Figure 8 shows the extension of the disordered micellar solution.

The volume fraction profiles of EO, PO, and H_2O for the H_1 phase are shown in Figure 9. It is clear that the interior of the rods is rich in the hydrophobic PO, whereas the outer parts consist of hydrated EO segments. At increasing temperature, the domain size increases and the volume fraction of the EO segments in the water region is reduced. The latter is a consequence of the reduced solubility as modeled by using internal degrees of freedom for EO. Since EO is not fully compatible with PO, the EO segments tends to form a new shell between the PO core and the continuous water region.

In the process of the determination of the most stable phase, the domain size of each phase is optimized. Figure 10 shows the predicted domain sizes for the equilibrium phases at two temperatures. Generally the domain sizes increase with increasing temperature. This is related to the smaller projected surface area for the PEO block due to the reduced solubility. Moreover, the domain size increases at transitions where the curvature is increased, but decreases within a phase as the polymer concentration is increased.

Most synthetic polymers are polydisperse. In the case of block copolymers, even a small polydispersity may profoundly affect the behaviour of the properties of the solution.

The lattice approach has been used to examine the effect of a polydisperse PEO-PPO-PEO triblock copolymer on the location of the cmc [39]. The polydisperse sample were represented by several components selected from the Schulz-Zimm distribution. Both the case of only a mass polydispersity and the case of mass-and-composition polydispersity were considered. Figure 11 shows how the location of the cmc changes as a function of the polydispersity ratio M_m/M_n for $(EO)_{37}(PO)_{56}(EO)_{37}$ triblock copolymer (Pluronic P105) in aqueous solution. Here M_m and M_n are the mass and number weighted mass averages, respectively. Depending on the criterion of the cmc (here the volume fraction of micelles in the solution is used) the cmc may change by several orders of magnitude already at the moderate polydispersity ratio of M_m/M_n= 1.3. Further investigations showed that the radial extension of the micelle *decreases* at increasing total polymer volume fraction due to the replacement of longer and less soluble polymer fractions with shorter and more soluble fractions [39]. Such observations have been made experimentally by Tuzar et al. [44] in a different system but the origin of the trends were never clarified.

It is straightforward to study the solubilization of lyophobic components in the center of the micelles [38,40,45]. One merely introduces an additional component with appropriate interaction parameters beside the block copolymer and the solvent. Figure 12 shows the radial volume fraction profiles for $(EO)_{30}(PO)_{61}(EO)_{30}$ triblock copolymer (Pluronic P104) in aqueous solution without and with a hydrophobic solute [40]. The model predicts that the solute is solubilized in the core of the micelle but tends to avoid the outer part of the core. Moreover,

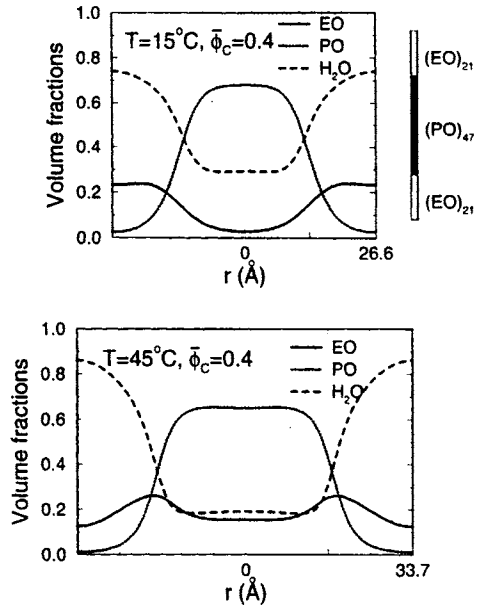

Figure 9. Radial volume fraction profiles of EO and PO segments and H_2O for the hexagonal phase of $(EO)_{21}(PO)_{47}(EO)_{21}$ in aqueous solution at two different temperatures at a total polymer volume fraction of 0.4. (Reprinted with permission from ref [32]. Copyright 1996 American Chemical Society.)

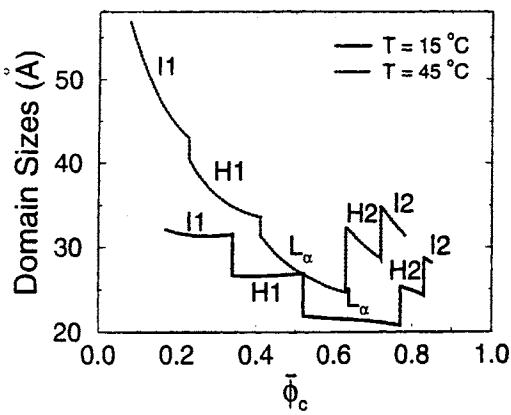

Figure 10. Domain sizes of the different equilibrium ordered phases for $(EO)_{21}(PO)_{47}(EO)_{21}$ in aqueous solution as a function of the polymer volume fraction at two different temperatures. (Reprinted with permission from ref [32]. Copyright 1996 American Chemical Society.)

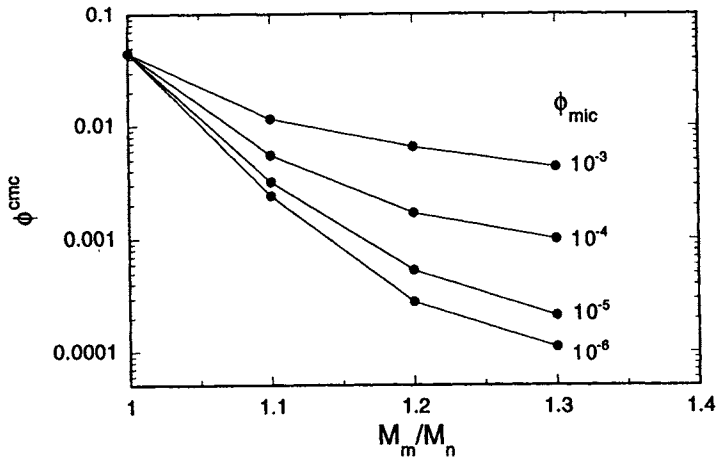

Figure 11. Critical micellar volume fraction as a function of the polydispersity ratio at different micellar volume fractions (criterion of the cmc) for $(EO)_{37}(PO)_{56}(EO)_{37}$ in aqueous solution at 320 K. The calculations were performed for a mass-polydisperse sample represented by 5 components. The symbols denote the calculated points, whereas the lines are given for increased readability. (Data from Linse [39].)

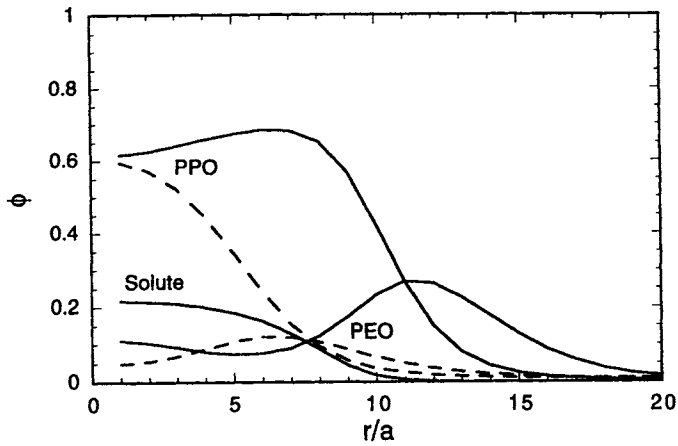

Figure 12. Radial volume fraction profiles of EO, PO, and solute for $(EO)_{30}(PO)_{61}(EO)_{30}$ in aqueous solution at 300 K without (dashed curves) and with (solid curves) solubilized hydrophobic solute at a polymer volume fraction $\phi_P = 0.05$. The volume fraction of the solute $\phi_{solute} = 2.9 \times 10^{-5}$ is close to its saturation point. (A full account of the other conditions are given by Hurter et al. [40]. Note, $kT\chi_{POp\text{-}POn}$ is erroneously given in Table III in ref [40]; it should be 1.4 kJ mol^{-1}.)

the micellar aggregation number increases from ca. 10 to ca. 55 and the increase of the micellar size is obvious from the profiles. Thus, the scaling, semi-analytic, and numerical mean-field approaches all predict a micellar growth upon solubilization.

5. SIMULATION APPROACHES

We will restrict the use of the word simulation to techniques such as Monte Carlo simulation and molecular dynamics. These methods provide us with a wealth of information of model systems by making full statistical mechanical averages over the relevant degrees of freedom. The methods are computationally intensive and have grown in parallel with the computer development. Simulation methods have been applied to polymeric systems as well to other molecular systems. A recent book edited by K. Binder serves as an excellent introduction to simulation techniques and how these are applied to different subfields of polymeric systems [46].

The simulation of polymers is inherently computationally demanding due to the slow rearrangement of the molecules and this is in particular accentuated when investigating non-local properties. In order to facilitate the enumeration of the conformations, lattice systems are frequently used. It is today still not possible to routinely make direct simulations of the self-assembly of long block copolymers. However, substantial effort has been devoted to the self-association into micelles and liquid crystalline phases of short chain molecules. These simulations have been performed either on a lattice or off-lattice with simple spring-bead models. Moreover, the structure and dynamics of single micelles as well as mono- and bilayers have been investigated with (nearly) fully atomistic models [47-49], but in these studies the simulations were started from already assembled systems.

5.1. Micellar structure and the cmc

Pratt and coworkers performed early Monte Carlo simulations of single micelles formed by a fixed number of A_3B and A_5B chains on a diamond lattice [50,51]. Rodrigues and Mattice made further investigations of the structure of micelles composed of $A_{10}B_{10}$ [52] and $A_5B_{10}A_5$ chains [53]. These studies showed that (i) the interfacial region between the two types of beads is significant and (ii) that the shape of the aggregate is not perfectly spherical. Thus, the simulation methods, like the numerical self-consistent mean-field methods, provide information on the thickness of the interfacial region between the two blocks, whereas the other approaches often neglect the interfacial thickness. Moreover, the strength of the simulation methods is that the shape of the aggregate is a result of the system parameters and that all relevant fluctuations are included.

Subsequent lattice [54-61] and off-lattice [62,63] simulations involved a larger number of chain molecules making it possible to establish an equilibrium among free unimers and several micelles of different size. Beside structural information, these more extended studies can provide information of the distribution function of the aggregation number and the cmc.

The self-assembly of the diblock "copolymer" $A_{10}B_{10}$ on a primitive cubic lattice with six interacting neighbours has been extensively investigated by Mattice and coworkers [52,56-58] and by Wijmans and Linse [59-61]. These studies gives a detailed picture of the micellization. Figure 13 clearly illustrates the plateau of the chemical potential of the chains as a function of

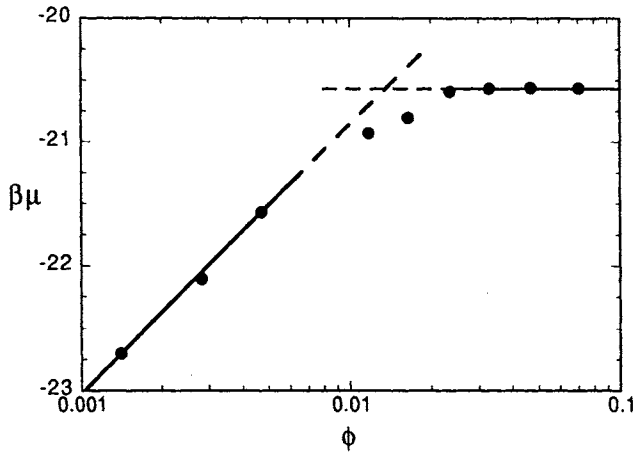

Figure 13. Chemical potential of $A_{10}B_{10}$ chains in solution as function of the volume fraction. Interaction energies: $w_{AB}/kT = w_{AS}/kT = 0.45$ and $w_{BS}/kT = w_{ii}/kT = 0$ (i = A, B, or S). (Data from Wijmans and Linse [61].)

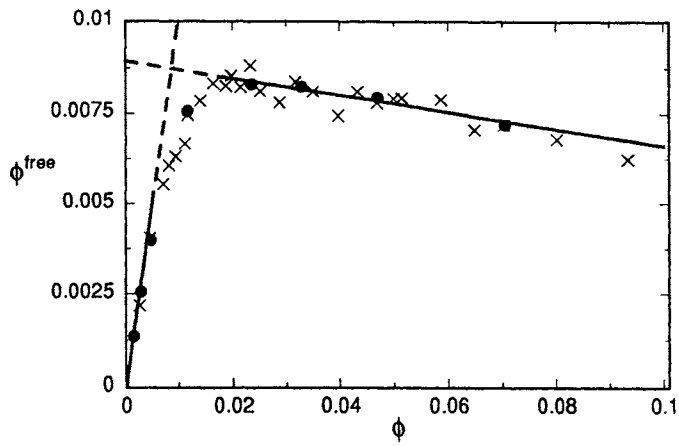

Figure 14. Volume fraction of free $A_{10}B_{10}$ chains in solution as a function of the volume fraction. Interaction parameters as in Figure 13. (Data from Wang et al. [56] (crosses) and Wijmans and Linse [61] (filled circles).)

the total volume fraction. The levelling off of the chemical potential is of course associated with the formation of micelles and the intersection of the extrapolated lines can be taken as the cmc. The volume fraction of free (non-associated) chains, ϕ^{free}, as a function of the total volume fraction is displayed in Figure 14. As for previous theories (cf. Figure 3), ϕ^{free} levels off when the micelles start to form. In fact, the simulation studies predict a reduction of ϕ^{free} at high micellar volume fractions. An extrapolation gives an estimate of the cmc in good agreement with that obtained from the chemical potentials. Figure 15 illustrates the bimodal distribution of aggregate sizes above the cmc as obtained from simulation. The solution is essentially composed by free chains, chains in small clusters composed by a few chains, and closed aggregates with ca. 20-40 chains. Additional analysis shows that micelles with an aggregation number of 30 are only weakly distorted toward a prolate shape from a spherical symmetry [59]. Similar characteristic micellar size distribution functions were also obtained from lattice simulations of short chain molecules by Desplat and Care [55], by Larson [64], and from extensive off-lattice simulations of eight bead long chain molecules with short range interactions by Smit et al.[63].

5.2. Ordered phases

A number of different lattice simulations have been performed to examine the ordered phases occurring in block copolymers solutions [64-73]. These studies cover chain lengths from 8 to almost 200 beads and deal with dilute as well as with more concentrated solutions with either a selective solvent, a nonselective solvent, or a binary solvent.

So far, close packed spheres of different cubic symmetries [65,66,69,71,72], hexagonally packed cylinders [64-66,69,71,72], the gyroidal structure [69], perforated lamellae [64-67,69,72], and lamellae [64-73], have been identified. Figure 16 shows a ternary phase diagram for the A_4B_4/A/B system obtained from lattice Monte Carlo simulations. Besides the extended classical lyotropic liquid crystalline phases, a narrow gyroidal phase was observed between the hexagonal and lamellar region. So far, it is not fully clear whether the gyroidal phase is a stable or only metastable phase [66]. In the disordered phases the simulation predicted an elongation of the micelles close to the to liquid crystalline phases, and the lamellar phase displayed perforations near the phase boundary toward the hexagonal phases. In such investigations, the size of the simulation box imposes nonphysical constrains on the domain sizes. This problem becomes less severe as the box length increases relative to the domain size. This influence has been systematically investigated for smaller chains as A_3B_3, A_4B_4, and A_3B_{12} [66].

The self-assembly and the concomitant microphase separation occurring in melts (as well as in nonselective solvents) are only driven by the interactions among the A and B segments themselves. However, lattice simulation of melts are technically difficult to perform, but by introducing vacancies, or equivalently, a nonselective solvent, it is possible to deal with melts and the effect of the the vacancies is taken account by a rescaling of the interaction parameter. Extensive simulations has been performed to investigate the critical χN and the stretching of the blocks of symmetric block copolymers. In particular, simulations [68,73], show that the order-disorder transition of block copolymer occurs at $\chi N > 11.5$ as predicted by mean-field theory in the limit of infinite chain lengths [74].

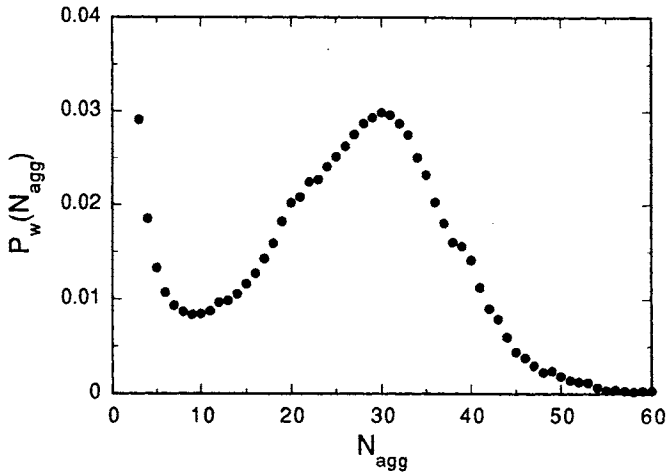

Figure 15. Normalized weight distribution of the aggregation numbers of micelles formed by $A_{10}B_{10}$ chains in solution at $\phi = 0.047$. The probability of free unimers is 0.17. Interaction parameters as in Figure 13. (Data from Wijmans and Linse [59].)

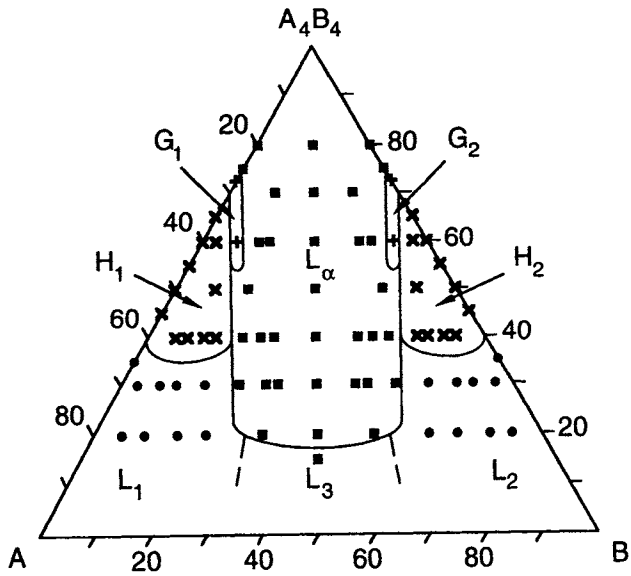

Figure 16. Ternary phase diagram for the A_4B_4/A/B system on a simple cubic lattice with 26 interacting neighbours with a contact energy $w_{AB}/kT = 0.1538$. L_1 and L_2 are disordered micellar phases, L_3 a disordered bicontinuous phase, H_1 and H_2 hexagonal phases, G_1 and G_2 gyroidal cubic phases, and L_α a lamellar phase. Only one half of the phase diagram was simulated, the rest is obtained by symmetry. (Data from Larson [69].)

6. CONCLUSIONS

The area of modelling block copolymers in solution is rapidly expanding and develops in close connection with the experimental progress. Some of the major approaches used to examine various aspects of the self-assembly of block copolymers in solution have been given. As we have seen, the development has been benefitted from the field of block copolymer melts and from the field of self-assembly of surfactants.

In brief, the scaling approach relies on a number of basic approximations which successively are relaxed in the more elaborated approaches. Typical for the scaling approach are the simple expressions relating a few variables describing the system which are obtained after a minimization of the free energy. In the semi-analytic mean-field models, the full functional dependencies among the variables are obtained, again, after a minimization of the free energy. Moreover, since a reference state is included, the theories are also able to predict the cmc, the micellar volume fractions etc, besides the aggregation number and the size of the micellar core and shell. The remaining two approaches are more fundamental in the sense that they explicitly contain chain molecules and that they are based on configurational averages. In the numerical self-consistent mean-field models, properties of the system are calculated for a given morphology. Volume fraction profiles appear as a results and are hence not a part of the assumption. In addition to the properties given above, predictions of the interfacial width and interfacial tension are made, and information on the distribution of individual segments is provided. Finally, in the simulation approaches, the mean-field approach is lifted and the morphology of the equilibrium structures is obtained directly. Furthermore, since fluctuations in all 3 dimensions are included, the results are improved over those from the numerical self-consistent mean-field models. However, (i) the simulation results are subjected to statistical uncertainty, (ii) the influence of boundary conditions, system size etc has to be assessed, and (iii) considerations of whether the system is in equilibrium or not has to be addressed.

Hence, the quality of the predictions are improved in the order that the types of approaches have been presented. Still, the scaling approach provides us with simple and very useful pictures of the system which is not the case for the more numerically intensive methods. Also, the computational effort increases in the same direction. Whereas the computer time is negligible for the minimization of the free energy in the semi-analytic mean-filed models (< 1 CPU second on a workstation), it is of the order of seconds or minutes for solving the set of non-linear equations obtained from the numerical self-consistent mean-field models. Finally, the computational effort for simulation of chain systems is of the order of days and upwards.

Nevertheless, the more computationally demanding approaches are expected to grow in importance. Fewer approximations are involved and a more detailed picture is provided. So far, most simulations have dealt with generic chains, but it is feasible to bring more chemistry into the models. An example illustrated here is the notion of internal degrees of freedom which makes it possible to model temperature dependent solvency from basic assumptions. This and similar approaches could be directly transferred into the models used in the simulation investigations. Another area of expected development is more complex models of the self-assembly of polyelectrolytes and ionomers. The increased number of system parameters and the computer intensive evaluation of the electrostatic interactions in direct simulations have, so far, hampered the progress here.

Finally, in practical all approaches, the short-range interaction are described by χ-

parameters or nearest neighbour interactions. In order to mimic some real system, suitable assignments have to be made. So far, the values of these parameters have been (i) estimated from more elaborate theories, (ii) extracted from simulation of small systems described on an atomic level, or (iii) obtained by fitting to experimental data. Due to the great simplification of the models, these parameters should be viewed as effective parameters with, at most, some physical relevance, making procedure (i) and (ii) less useful. This is, e.g., illustrated by Figure 6 where two different theories gives strongly different cmc for the same χ-value. The reason is of course (i) that these terms in which the χ-parameter enter are different, and (ii) these terms are balanced by other free energy terms which depend on the type of theory. The unrealistically low cmc $\phi \approx 10^{-34}$ for PEO-PPO diblock copolymer with 70% PEO as obtained by Nagarajan and Ganesh [21] by using χ-parameter from other sources constitutes a second example. Thus, it is clear that χ-parameters are not generally transferable between the different types of theories and there is also no guaranty of transferablilty between different applications of the same theory/model. However, our own experience is that for EO- and PO-containing polymers in aqueous solution, we have successfully been able to gradually build up values of χ-parameters from simpler system and employ those in more complex ones in a fruitful manner. In this scheme, phase diagrams of the binary PEO/water system were used to fit the values of the internal state parameters of EO and the $\chi_{EO,water}$-parameters (there are several parameters due to the presence of internal states) [34] and similarly for PPO in water [35]. Thereafter, interaction parameters between the EO and PO segments were fitted by using phase diagrams of the ternary PEO/PPO/water system and the previous obtained values from the binary systems [75]. Finally, the full set of parameters was used to predict a number of different properties of PEO-PPO-PEO triblock copolymers at different conditions with satisfactorily predictive power [32,36-39].

Acknowledgements

It is a pleasure to thank J. Noolandi, A.-C. Shi, and C. Wijmans for pleasant and fruitful collaboration and their permission to shown some of our recent research results. It is also a great pleasure to thank P. Alexandridis and L. Piculell for their kind and useful comments on the manuscript.

REFERENCES

1. M.W. Matsen and F.S. Bates, Macromolecules, 29 (1996) 1091.
2. P.G. de Gennes, in Solid State Physics, Ed L. Liebert, Academic, New York, 1978, suppl. 14.
3. A. Halperin, Macromolecules, 20 (1987) 2943.
4. C. Marques, J.-F. Joanny, and L. Leibler, Macromolecules, 21 (1988) 1051.
5. M. Daoud and J.P. Cotton, J. Phys (Paris) 43 (1982) 531.
6. T.M. Birshtein and E.B. Zhulina, Polymer, 25 (1984) 1453.
7. P.G. de Gennes, Scaling Concepts in Polymer Physics, Cornell University Press, Ithaca, N.Y., 1979.
8. R. Nagarajan and K. Ganesh, J. Chem. Phys., 98 (1993) 7440.
9. N. Dan and M. Tirrell, Macromolecules, 26 (1993) 4310.

10. L. Leibler, H. Orland, and J.C. Wheeler, J. Chem. Phys. 79 (1983) 3550.
11. M.R. Munch and A.P. Gast, Macromolecules, 21 (1988) 1360.
12. J. Noolandi and K.M. Hong, Macromolecules, 16 (1983) 1443.
13. M.G. Whitmore and J. Noolandi, Macromolecules, 18 (1985) 657.
14. P.J. Flory, Principles of Polymer Chemisty, Cornell University Press, Ithaca, N.Y., 1953.
15. E. Helfand and Y. Tagami, J. Polym. Sci. Part B, 9 (1971) 741.
16. G. ten Brinke and G. Hadziioannou, Macromolecules, 20 (1987) 486.
17. N.P. Balsara, M. Tirrell, and T.P. Lodge, Macromolecules, 24 (1991) 1975.
18. O. Procházka, Z. Tuzar, and P. Kratochvíl, Polymer, 32 (1991) 3038.
19. W. Zheng, Z.-G. Wang, Macromolecules, 28 (1995) 7215.
20. V. Abetz, R. Stadler, L. Liebler, Polymer Bulletin, 37 (1996) 135.
21. R. Nagarajan and K. Ganesh, J. Chem. Phys., 90 (1989) 5843.
22. A. Gao and A. Eisenberg, Macromolecules, 26 (1993) 7353.
23. D.F. Shim, C.M. Marques, and M. E. Cates, Macromolecules, 24 (1991) 5309.
24. P. Sens, C. M. Marques, and J.-F. Joanny, Macromolecules, 26 (1996) 4880.
25. R. Nagarajan and K. Ganesh, Macromolecules, 22 (1989) 4312.
26. R. Nagarajan and K. Ganesh, J. Colloid Inteface Sci., 184 (1996) 489.
27. J.F. Marko and Y. Rabin, Macromolecules, 25 (1992) 1503.
28. J.M.H.M. Scheutjens and G.J. Fleer, J. Phys. Chem., 83 (1979) 1619.
29. G.J. Fleer, M.A. Cohen Stuart, J.M.H.M. Scheutjens, T. Cosgrove, and B. Vincent, Polymer at Interfaces, Champan & Hall, London, 1993.
30. M. Doi and S.F. Edwards, The Theory of Polymer Dynamics, Clarendon Press, Oxford, 1986.
31. K.M. Hong and J. Noolandi, Macromolecules, 14 (1981) 727.
32. J. Noolandi, A.-C. Shi, and P. Linse, Macromolecules, 29 (1996) 5907.
33. O.A. Evers, J.M.H.M. Scheutjens, and G.J. Fleer, Macromolecules, 23 (1990) 5221.
34. G. Karlström, J. Phys. Chem., 89 (1985) 4962.
35. P. Linse and M. Björling, Macromolecules, 24 (1991) 6700.
36. P. Linse, Macromolecules, 26 (1993) 4437.
37. P. Linse, J. Phys. Chem., 97, (1993) 13896.
38. P. Linse, Macromolecules, 27 (1995) 2685.
39. P. Linse, Macromolecules, 27 (1995) 6404.
40. P.N. Hurter, J.M.H.M. Scheutjens, and T.A. Hatton, Macromolecules, 26 (1993) 5030.
41. R. Israëls, F.A.M. Leermakers, and G.J. Fleer, Macromolecules, 27 (1994) 3087.
42. F.A.M. Leermakers, C.M. Wijmans, G.J. Fleer, Macromolecules, 28 (1995) 3434.
43. D. G. Hall and B.A. Pethica. In Nonionic Surfactants, Ed. M.J. Schick, Marcel Dekker, New York, 1976.
44. Z. Tuzar, P. Stepánek, C. Konák, and P. Kratochvíl, J. Colloid Interface Sci., 105 (1985) 372.
45. P.N. Hurter, J.M.H.M. Scheutjens, and T.A. Hatton, Macromolecules, 26 (1993) 5592.
46. K. Binder, Monte Carlo and Molecular Dynamics Simulations in Polymer Science, Oxford University Press, New York, 1995.
47. B. Jönsson, O. Edholm and O. Teleman, J. Chem. Phys, 85 (1986) 2259.
48. K. Watanabe, M. Ferrario and M.L. Klein, J. Phys. Chem., 92 (1988) 819.
49. E. Egberts, H.J.C. Berendsen, J. Chem. Phys., 89 (1988) 3718.

50. S.W. Haan and L.R. Pratt, Chem. Phys. Lett., 79 (1981) 436.
51. B. Owenson and L.R. Pratt, J. Phys. Chem., 88 (1984) 2905.
52. K. Rodrigues and W.L. Mattice, J. Chem. Phys., 95 (1991) 5341.
53. K. Rodrigues and W.L. Mattice, Langmuir, 8 (1992) 456.
54. D. Brindle and C. M. Care, J. Chem. Soc. Faraday Trans., 88 (1992) 2163.
55. J.-C. Desplat and C. M. Care, Mol. Phys., 87 (1996) 441.
56. Y. Wang, W.L. Mattice and D.H. Napper, Langmuir, 9 (1993) 66.
57. Y. Zhan and W.L. Mattice, Macromolecules, 27, (1994) 677.
58. P. Adriani, Y. Wang, and W.L. Mattice, J. Chem. Phys. 100 (1994) 7718.
59. C.W. Wijmans and P. Linse, Langmuir, 11 (1995) 3748.
60. C.W. Wijmans and P. Linse, J. Phys. Chem., 100 (1996) 12583.
61. C.W. Wijmans and P. Linse, J. Chem. Phys., 106 (1997) 328.
62. B. Smith, P.A.J. Hilbers, K. Esselink, L.A.M. Rupert, M.N. van Os, and A.G. Schlijper, J. Phys. Chem., 95 (1991) 6361.
63. B. Smith, K. Esselink, P.A.J. Hilbers, M.N. van Os, L.A.M. Rupert, and I. Szleifer, Langmuir, 9 (1993) 9.
64. R.G. Larson, J. Chem. Phys., 96 (1992) 7904.
65. R.G. Larson, J. Chem. Phys., 91 (1989) 2479.
66. R.G. Larson, Chem. Eng. Sci., 49 (1994) 2833.
67. R.G. Larson, Mol. Sim., 13 (1994) 321.
68. R.G. Larson, Macromolecules, 27 (1994) 4198.
69. R.G. Larson, J. Phys. II (Paris) 6 (1996) 1441.
70. L.A. Molina, A. López Radríges and J.J. Freire, Macromolecules, 27 (1994) 1160.
71. L.A. Molina and J.J. Freire, Macromolecules, 28 (1995) 2705.
72. M.B. Ko and W.L. Mattice, Macromolecules, 28 (1995) 6871.
73. H. Fried and K. Binder, J. Chem. Phys., 94 (1991) 8349.
74. L. Leibler, Macromoleucles, 13 (1980) 1602.
75. M. Malmsten, P. Linse, K.-W. Zhang, Macromolecules, 26 (1993) 2905.